Photoconductivity studies of gold nanoparticles supported on amorphous and crystalline TiO_2 matrix prepared by sol-gel method

G. Valverde-Aguilar, J.A. García-Macedo, and V. Renteria-Tapia,
Departamento de Estado Sólido, Instituto de Física, Universidad Nacional Autónoma de México,
Apartado Postal 20-364 México, D.F., 04510, México,
Tel. (5255) 56225103; Fax (5255) 56161535
E-mail: valverde@fisica.unam.mx

M. Aguilar-Franco
Departamento de Física Química. Instituto de Física, Universidad Nacional Autónoma de México,
Apartado Postal 20-364 México, D.F., 04510, México.

Recibido el 7 de diciembre de 2009; aceptado el 13 de julio de 2010

Gold metallic nanoparticles embedded in amorphous and crystalline TiO_2 matrix as powders and films were synthesized by the sol–gel process at room temperature. The TiO_2 matrix was synthesized by using tetrabutyl orthotitanate as the inorganic precursor. The films were spin-coated on glass wafers. The samples were annealed at at 100°C for 30 minutes and sintered at 520°C for 1 hour to generated anatase and rutile phases. The film shows a light blue colour. The amorphous film exhibits an absorption band at 568 nm. The crystalline film exhibit two absorption peaks located at around 402 (from TiO_2 matrix) and 651 nm is due to the surface plasmon resonance of the gold nanoparticles. The films were studied using X-ray diffraction, infrared spectroscopy, scanning electron microscopy, high resolution transmission electronic microscopy and UV-Vis absorption spectroscopy. Photoconductivity studies were performed on amorphous and crystalline TiO_2/Au films. The experimental data were fitted with straight lines at darkness and under illumination at 515 nm and 645 nm. This indicates an ohmic behavior. Transport parameters were calculated.

Keywords: Titania; gold nanoparticles; sol-gel; photoconductivity; Gans theory; refractive index.

Nanopartículas metálicas de oro insertadas en una matriz de TiO_2 (amorfa y cristalina) fueron sintetizadas en forma de polvos y películas por el método sol-gel a temperatura ambiente. La matriz de TiO_2fue sintetizada usando el tetrabutil ortotitanato como precursor inorgánico. Las películas fueron depositadas por spin-coating sobre substratos de vidrio. Las muestras fueron recocidas a 100°C por 30 minutos y sinterizadas a 520°C por 1 hora para generar las fases cristalinas anatasa y rutilo. Estas películas cristalinas muestran un color azul, y su absorción está en 645 nm, la cual es debido a su plasmón de resonancia. Las películas fueron caracterizadas por difracción de rayos X, espectroscopia infrarroja, microscopia de barrido y de alta resolución. Los estudios de fotoconductividad fueron realizados en las muestras amorfas y cristalinas de TiO_2/Au. Los datos experimentales obtenidos en la oscuridad y bajo iluminación a 515 nm y 645 nm fueron ajustados por mínimos cuadrados. Esto indica un comportamiento óhmico. Los parámetros de transporte fueron calculados.

Descriptores: Titanio; Nanopartículas metálicas de oro; sol-gel; películas delgadas; fotoconductividad; teoría de Gans; índice de refracción.

PACS: 72.80.-r; 73.61.-r

1. Introduction

Titanium dioxide (TiO_2) is a non-toxic material. TiO_2 thin films exhibit high stability in aqueous solutions and no photocorrosion under band gap illumination and special surface properties. TiO_2 thin films are already widely used in the study of the photocatalysis and photoelectrocatalysis of organic pollutants [1,2]. Photoelectrocatalytic system has received a great deal of attention due to drastically enhanced quantum efficiency [3]. By applying small bias, recombination of generated electron–hole pairs is retarded.

TiO_2 is the subject of intensive research, especially with regard to its end uses in solar cells, chemical sensors, photoelectrochemical cells, photocatalysis and electronic devices [4,5]. Due to its wide-ranging chemical and physical properties (electrical conductivity, photosensitivity, and aqueous environments) TiO_2 has a large variety of potential applications. As a wide band gap semiconductor, TiO_2 shows a diverse heterogeneity of crystalline phases, whereby it is possible to find it in anatase, rutile or brookite form [6].

TiO_2 are almost impossible to measure in great detail in powder form, due to the difficulty in manipulating grain sizes in the range of 1–50 nm [7]. Furthermore, measurements carried out on powder represent only an average value for many grains oriented in all possible directions. This difficulty in working with powder samples, together with the ongoing search for new applications, has compelled many researchers to work with TiO_2 thin films instead.

In the present work, we described the synthesis, characterization and photoconductivity behaviour of amorphous and crystalline TiO_2 films doped with gold nanoparticles (NP's). The films were produced by the sol–gel process at room temperature by using the spin-coating method and deposited on glass wafers. The samples were sintered at 520°C for 1 hour. The obtained films were studied by X-ray diffraction (XRD), optical absorption (OA), infrared spectroscopy (IR), scanning electron microscopy (SEM) and transmission electron microscopy (TEM) studies. Photoconductivity studies were performed on these films. Transport parameters were calculated.

2. Experimental

Glass substrates were cleaned in boiling acidic solution of sulphuric acid-H_2O_2 (4:1) under vigorous stirring for 30 minutes. They were then placed in deionized water and boiled for 30 minutes, rinsed three times with deionized water and stored in deionized water at room temperature.

Preparation of TiO_2 *solution.* All reagents were Aldrich grade. The precursor solutions for TiO_2 films were prepared by the following method. Tetrabutyl orthotitanate and diethanolamine ($NH(C_2H_4OH)_2$) which prevent the precipitation of oxides and stabilize the solutions were dissolved in ethanol. After stirring vigorously for 2 h at room temperature, a mixed solution of deionized water and ethanol was added dropwise slowly to the above solution with a pipette under stirring. Finally, Tetraethyleneglycol (TEG) was added to the above solution. This solution is stirred vigorously to obtain a uniform sol. The resultant alkoxide solution was kept standing at room temperature to perform hydrolysis reaction for 2h, resulting in the TiO_2sol.

Preparation of Au stock solution. 0.03 M of Hydrogen Tetrachloroaurate(III) hydrate ($HAuCl_4$·aq) was dissolved in a mixture of deionized water and ethanol. It was stirred for 5 minutes.

The Au stock solution was added to 20 ml of TiO_2 solution. This final solution was stirred for 17 hours at room temperature to obtain a purple colour. The final chemical composition of this solution was $Ti(OC_4H_9)_4$: $NH(C_2H_4OH)_2$: C_2H_5OH : DI H_2O : TEG: nitric acid: $HauCl_4$ = 1:1: 14.1:1:1.028:0.136:0.024. The TiO_2 with gold NP's solution has a pH = 6.0. The TiO_2 films were deposited by the spin-coating technique. The precursor solution was placed on the glass wafers (2.5×2.5 cm^2) using a dropper and spun at a rate of 3000 rpm for 20 s.

After coating, the film was dried at 100°C for 30 min in a muffle oven and sintered at 520°C for 1 h in a muffle oven in order to remove organic components. The procedure was repeated two times to achieve the film thickness with two layers. The crystalline films show a light blue colour.

UV-vis absorption spectra were obtained on a Thermo Spectronic Genesys 2 spectrophotometer with an accuracy of ±1 nm over the wavelength range of 300-900 nm. The structure of the final films was characterized by XRD patterns. These patterns were recorded on a Bruker AXS D8 Advance diffractometer using Ni-filtered CuKα radiation. A step-scanning mode with a step of 0.02° in the range from 1.5 to 60° in 2θ and an integration time of 2 s was used. IR spectra were obtained from a KBr pellet using a Bruker Tensor 27 FT-IR spectrometer. Pellets were made from a finely ground mixture of the sample and KBr at a ratio of KBr:sample = 1:0.019. The thickness of the films was measured using a SEM microscopy Model STEREOSCAN at 20 kV.

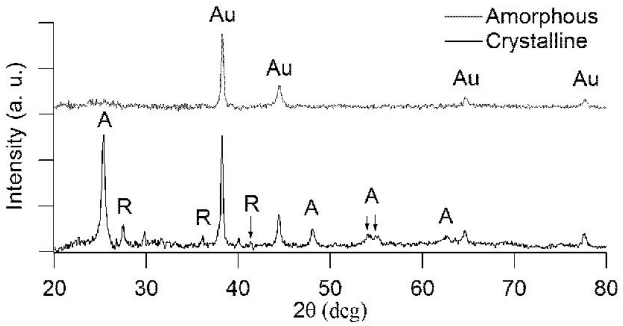

FIGURE 1. X-ray diffraction pattern at high angle of the amorphous and crystalline TiO_2 films with gold NP's.

For photoconductivity studies [8] silver electrodes were painted on the sample. It was maintained in a 10^{-5} Torr vacuum cryostat at room temperature in order to avoid humidity. For photocurrent measurements, the films were illuminated with light from an Oriel Xe lamp passed through a 0.25 m Spex monochromator. Currents were measured with a 642 Keithley electrometer connected in series with the voltage power supply. The applied electrostatic field E was parallel to the film. Light intensity was measured at the sample position with a Spectra Physics 404 power meter.

3. Results and discussion

3.1. X-ray diffraction patterns

The X-ray diffraction patterns of the amorphous and crystalline TiO_2 films with gold NP's is presented in Fig. 1.

From amorphous film, its spectrum reveals the presence of gold NP's by the diffraction peaks located at 2θ = 38.24, 44.39, 64.62 and 77.60 which can be indexed as (111), (200), (220) and (311) respectively. The position of the diffraction peaks is in good agreement with those given in ASTM data card (#04-0784).

The crystalline film sintered at 520°C for 1 hour exhibits very good crystallization that corresponds to anatase and rutile phases. The anatase phase was identified by the diffraction peaks located at 2θ = 25.33, 47.97, 54.00, 55.16 and 62.71 which can be indexed as (101), (200), (105), (211) and (204) respectively. The rutile phase was identified by the diffraction peaks located at 2θ = 27.47, 36.14 and 41.32 which can be indexed as (110), (101) and (111) respectively. The position of the diffraction peaks in the film is in good agreement with those given in ASTM data card (#21-1272) for anatase and ASTM data card (#21-1276) for rutile. The presence of gold NP's was detected by the same diffraction peaks identified in the amorphous film.

The average crystalline size (D) was calculated from Scherrer's formula [9] by using the diffraction peak (101) for anatase phase and the peak (110) for rutile phase:

$$D = \frac{0.9\lambda}{B\cos\theta} \tag{1}$$

with λ=1.54056$\times10^{-10}$m.

TABLE I. Summary of nanoscopic characteristics of amorphous and crystalline TiO_2/Au films.

Phase	B	Radian	D (nm)	Crystal phase (wt%)
Anatase (101)	0.44°	0.00768	18.5	59.7±4
Rutile (110)	0.31°	0.00543	26.3	37.4±3
Au	-	-	-	2.9±4

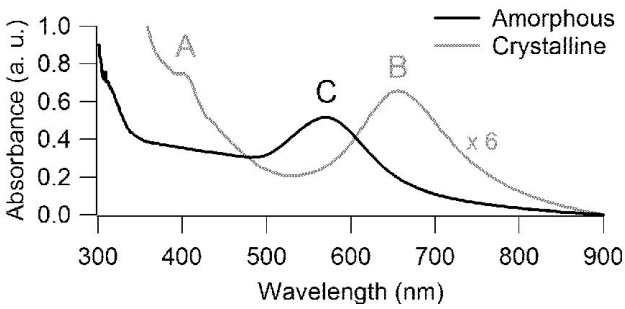

FIGURE 2. Absorption spectra of the amorphous (black solid line) and crystalline (grey solid line) TiO_2 film with gold NP's.

The percentage of anatase, rutile and gold phases was calculated by means of a Rietvield refinement. These calculations are shown in Table I.

3.2. Optical absorption

Figure 2 shows the optical absorption spectra of the amorphous and crystalline TiO_2/Au films taken at room temperature in the range of 300-900 nm. The spectrum of the film calcined at 450°C for 15 min shows an absorption band A located at 402 (3.08 eV) corresponding to the TiO_2 matrix, and a second band B located 651 nm (1.93 eV) corresponding to the surface plasmon resonance (SPR) of the gold NP's.

The spectrum of the amorphous film shows a peak shoulder C at 568 nm (2.68 eV) which is the SPR band of spherical Au nanoparticles [10,11].

To clarify the XRD and optical absorption experimental results, the formation mechanism of Au nanoparticles is discussed below. It is known that the photolysis of $HAuCl_4$ to the Au atom, Au^0, is a multiphoton event [12,13], and it proceeds by irradiation. Therefore, for amorphous TiO_2/Au film, the Au nucleation was slow and random because the $HAuCl_4$ ions were reduced by daylight (containing a little UV light) and this mostly happened after the gelation. The nuclei were thus distributed randomly within the TiO_2 skeleton and consequently led to the growth of the Au particles that were inhomogeneous, and their size distribution very wide.

Literature [8,14] reports an absorption peak for surface plasmon resonance (SPR) of gold nanoparticles around 500-550 nm. A red-shift in the maximum in absorbance towards larger wavelength (from 568 to 651 nm) with respect to the amorphous TiO2 film is evident as well as a broadening of the peak absorption width compared to the amorphous film.

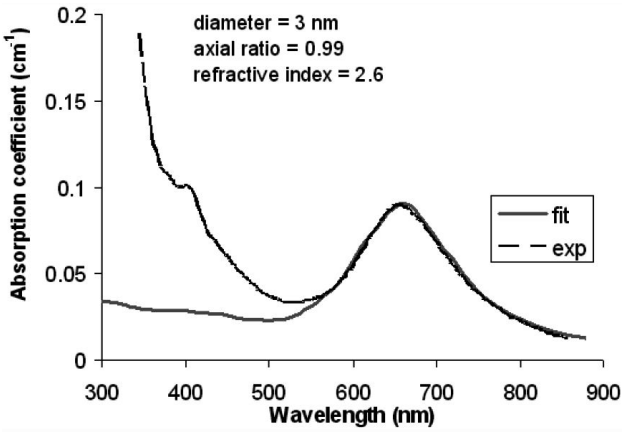

FIGURE 3. Experimental optical absorption spectrum (black dotted line) of the crystalline TiO_2/Au film. The calculated optical absorption spectrum (grey solid line) obtained by Gans theory.

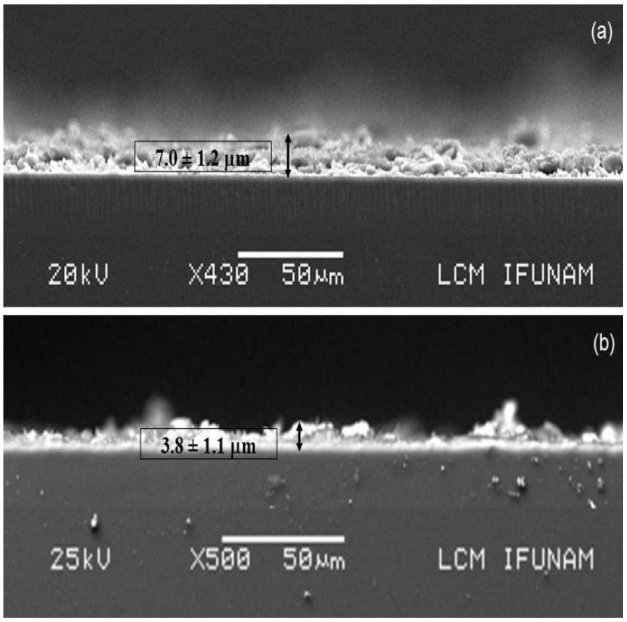

FIGURE 4. Cross-sectional SEM image of (a) amorphous and (b) crystalline TiO_2 films with gold NP's.

The dependence of this shift on the embedding medium indicates the high sensitivity of surface plasmon band to cluster-matrix interface properties. This fact is originated to the increase in the diameter of Au nanoparticles and an increment of the refractive index of TiO_2 matrix with increasing the heat-treatment temperature [15,16].

It is well known that the refractive index of TiO_2 films is related to the crystal phase (anatase or rutile), the crystalline size and the densities of the films [17]. For these reasons, the optical absorption spectrum (Fig. 2) was fitted very well using Gans theory [18] with a local refractive index n_{local} = 2.6 (Fig. 3). This index has a value close to the refractive index reported for the anatase phase ($n_{anatase}$= 2.54) [19]. This is consistent with the fact we have anatase phase in a proportion of 59.7 wt% according to the X-ray diffraction pattern

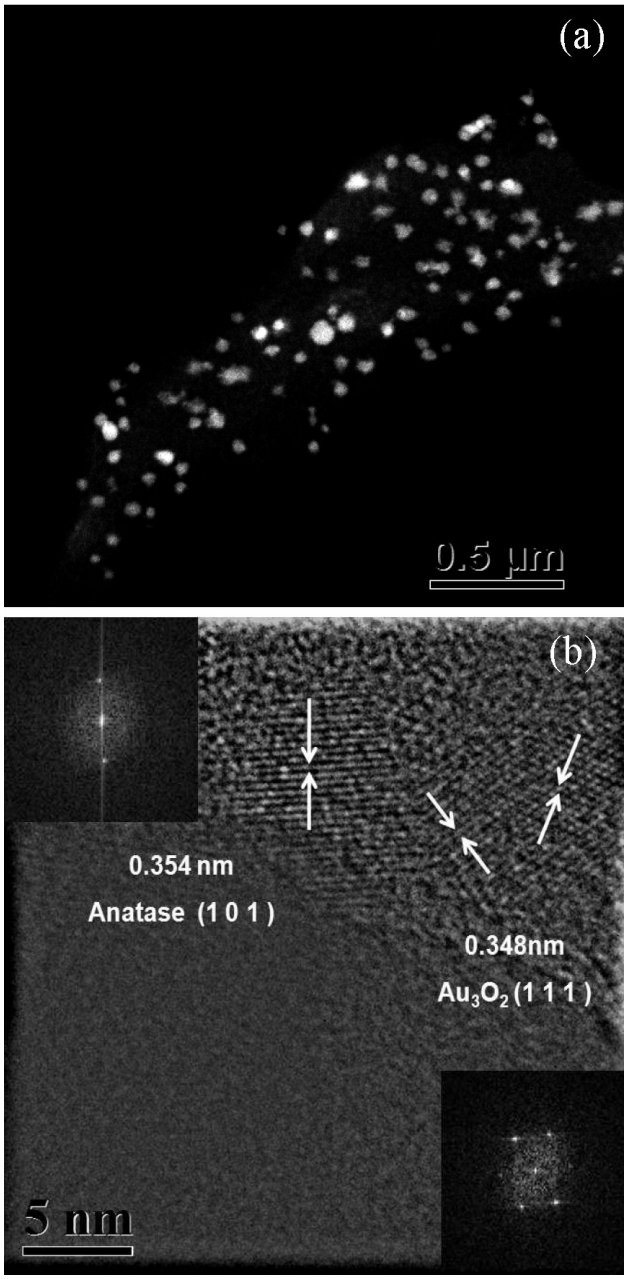

FIGURE 5. (a) HRTEM image of the crystalline TiO_2/Au film exhibits several gold NP's. (b) The reflections correspond to anatase nanocrystals and gold metallic nanoparticles were identified with white arrows. The inset shows the diffraction pattern showing these reflections.

(Fig. 3), while the rutile phase (n_{rutile} = 2.75) [20] has a proportion of 37.4 wt%.

3.3. SEM and HRTEM measurements

The thickness of the films was measured by SEM technique. Figure 4 shows the SEM image for amorphous and crystalline TiO_2 films with gold NP's. The thickness and the standard deviation for both kinds of films were calculated. The average thickness for amorphous and crystalline TiO_2/Au films is equal to 7.0 $\pm$ 1.2 μm and 3.8 $\pm$ 1.1 μm, respectively.

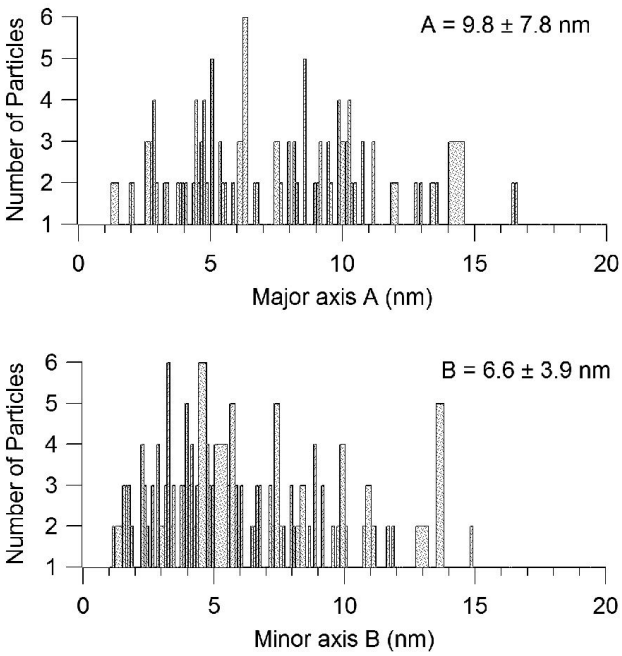

FIGURE 6. Size-distribution histograms obtained by HRTEM analysis of gold metallic NP's.

Figure 5 shows the HRTEM image of the crystalline TiO_2/Au film. Figure 5a shows gold NP's which were identified as brilliant particles.

Figure 4a shows a superposition of these populations. The reflection (101) corresponds to the anatase phase; and the reflection (111) corresponds to gold nanoparticle. The diffraction patterns (in the insert of the figure) show these reflections.

From HRTEM studies taking into account a population of gold NP's, the corresponding size-distribution histograms were obtained (Fig. 6). The distributions from the major axis A and minor length axis B and their respective standard deviations are A = 9.8 $\pm$ 7.8 nm (Fig. 5 a), B = 6.6 $\pm$ 3.9 nm.

3.4. Photoconductivity studies

Usually [8] Ohm's law under light illumination is given by

$$\vec{J} = \vec{J}\,ph + (\sigma_d + \sigma_{ph})\,\vec{E} \qquad (2)$$

TABLE II. Linear fittings of amorphous and crystalline TiO_2 films.

λ (nm)	TiO_2/ Au film	A_1	J_0
645	Crystalline	3.14×10^{-7}	1.40×10^{-3}
	Amorphous	5.36×10^{-10}	2.89×10^{-6}
515	Crystalline	3.64×10^{-7}	1.07×10^{-3}
	Amorphous	4.97×10^{-10}	2.27×10^{-6}
Darkness	Crystalline	3.73×10^{-7}	6.66×10^{-4}
	Amorphous	3.32×10^{-10}	1.89×10^{-6}

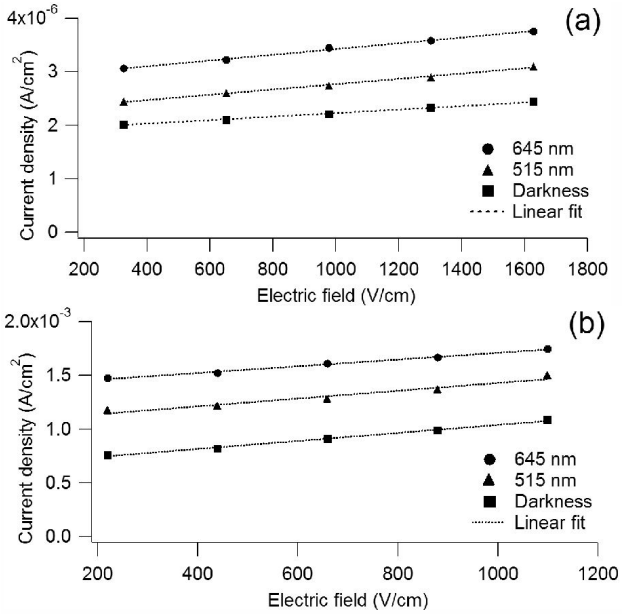

FIGURE 7. Experimental data of current density vs. electric field spectra from (a) amorphous and (b) crystalline TiO_2/Au films. Linear fits correspond to the dotted lines.

where $\vec{J}\,ph$ is the photovoltaic current density, and σ_{ph} is the photoconductivity. When the current densities are assumed to be parallel to the electric field $\vec{E}$ Eq. (2) becomes into the next one:

$$J = \frac{q\phi l_0 \alpha I}{h\nu} + \left(\sigma_d + \frac{q\phi\mu\tau\alpha I}{h\nu}\right) E \qquad (3)$$

with ϕ as the quantum yield of charge carrier photogeneration, l_0 as the charge carrier mean free path, α as the sample absorption coefficient, I as the light intensity at the frequency ν of illumination, h as the Planck's constant, and τgs the charge carriers mean lifetime. The first term is the photovoltaic transport effect, the second one is the dark conductivity σ_d =en$_0\mu$, and the third one is the photoconductivity itself.

Eq. (3) can be written as:

$$J = A_1 E + J_0 \qquad (4)$$

From the absorption spectrum of crystalline film (Fig. 2), the illumination wavelength for photoconductivity studies were chosen: 645 nm that corresponds to the maximum absorption band and 515 nm were there is no absorption. Photoconductivity results of amorphous and crystalline TiO_2 films with gold NP's are shown in Fig. 7. Current density as function of electric applied field on the film was plotted. The experimental data were fitted by least-squares with straight lines at darkness and under illumination. This indicates an ohmic behaviour. The linear fits are shown in Table II.

For both kinds of TiO_2/Au films, when the illumination wavelength decreases the J_0 value decreases. For crystalline film, when the illumination wavelength decreases, the slopeA_1 increases. It indicates a strong photoconductive behavior in these films.

TABLE III. ϕl_0 and $\phi\mu\tau$ parameters of amorphous and crystalline TiO_2/Au films.

λ (nm)	Parameters	Amophous TiO_2/ Au	Crystalline TiO_2/ Au
515	ϕl$_0$ (cm)	1.23×10^{-6}	1.41×10^{-3}
	$\phi\mu\tau$ (cm^2/V)	5.42×10^{-10}	3.42×10^{-8}
645	ϕl$_0$ (cm)	1.91×10^{-6}	9.71×10^{-4}
	$\phi\mu\tau$ (cm^2/V)	3.91×10^{-10}	7.87×10^{-8}

With the Eq. (3), by measuring I, the dark conductivity and the conductivity under illumination at 645 and 355 nm, and fitting the experimental data by the least squares method, as it is shown in Fig. 7, the photoconductive ($\phi\mu\tau$) and photovoltaic (ϕl_0) parameters were obtained by using the next expressions.

$$\phi l_0 = \left(J_{0_i} - J_{o_d}\right) \frac{h\,c}{e\alpha\lambda I}$$

$$\phi\mu\tau = \left(A_{1_i} - A_{1_d}\right) \frac{h\,c}{e\alpha\lambda I}$$

the subscripts i= illumination and d= darkness. Table III contains the ϕl_0 and $\phi\mu\tau$ values.

ϕl$_0$ and $\phi\mu\tau$ parameter values are bigger for crystalline films than those from amorphous ones. This indicates a strong photoconductive effect in the crystalline TiO_2/Au films.

4. Conclusions

High optical quality crystalline TiO_2 films with gold NP's were obtained by sol-gel process. XRD measurements reveal the presence of the anatase and rutile phases, which were produced after sintering treatment of 520°C for 1h. The anatase phase has a bigger proportion (59.75 wt%) than the rutile phase (37.4 wt%).

The optical absorption spectrum was fitted very good using Gans theory by using a local refractive index n$_{local}$ = 2.6. This index is related to the major crystal phase, anatase.

The experimental data J vs E were fitted by straight lines corresponding to an ohmic behaviour. Crystalline TiO_2/Au films exhibit a strong photoconductive effect. Anatase phase leads a better conduct on the electron/hole pair than the amorphous phase.

Acknowledgments

The authors acknowledge the financial supports of CONACYT 79781, REdNyN, PUNTA and PAPIIT IN107510. The authors are thankful to Luis Rendón (HRTEM), Roberto Hernández-Reyes (SEM) and Diego Quiterio (preparation of the samples for SEM studies) for technical assistance. GVA is grateful for CONACYT support.

1. R. Suarez, P.K. Nair, and P.V. Kamat, *Langmuir* **14** (1998) 3236.
2. Y. Shaogui *et al.*, *Phys. Chem. Chem. Phys.* **6** (2004) 659.
3. D.W. Kim *et al.*, *International Journal of Hydrogen Energy* **32** (2007) 3137.
4. C. Graziani Garcia, N-Y. Murakami R. Argazzi, and C.-A. Bignozzi, *J. Photochem. Photobiol. A: Chem.* **115** (1998) 239.
5. S. Dueñas *et al.*, *Semicond. Sci. Technol.* **20** (2005) 1044.
6. L. Hu, T. Yoko, H. Kosuka, and S. Sakka, *Thin Solid Films* **219** (1992) 18.
7. H. Gerischer, and A. Heller, *Electrochem. Soc.* **139** (1992) 113.
8. J. García Macedo, A. Mondragón, J.M. Hernández, and J.L. Maldonado, *Opt. Mat.* **3** (1994) 61.
9. G.J. Wilson *et al.*, *Langmuir* **22** (2006) 2016.
10. M.G. Manera *et al.*, *Sensors and Actuators B* **132** (2008) 107.
11. R.S. Sonawane, and M.K. Dongare, *Journal of Molecular Catalysis A: Chemical* **243** (2006) 68.
12. W. Shen, F.G. Liu, J. Qiu, and B. Yao, *Nanotechnology* **20** (2009) 105605.
13. K. Kurihara, J. Kizling, P. Stenius, and J.H. Fendler, *J. Am. Chem. Soc.* **105** (1983) 2574.
14. J. Yu, L. Yue, S. Liu, B. Huang, and X. Zhang, *J. Colloid and Interf. Sci.* **334** (2009) 58.
15. A. Ito, H. Masumoto, and T. Goto, *Materials Transactions* **44** (2003) 1599.
16. L.M. Liz-Marzán, M. Giersig, and P. Mulvaney, *Langmuir* **12** (1996) 4329.
17. C.J. Brinker, G.C. Frye, A. J. Hurd, and C.S. Ashley, *Thin Solid Films* **201** (1991) 97.
18. V.M. Rentería, and J. García–Macedo, *Colloids and Surfaces A: Physicochemical and Engineering Aspects* **278** (2006) 1.
19. Z. Wang, U. Helmersson, and P.-O. Käll, *Thin Solid Films* **405** (2002) 50.